*Met. Mater. Int., Vol. 18, No. 3 (2012), pp. 433~438*
doi: 10.1007/s12540-012-3008-0

# Kinetic Models of Controllable Pore Growth of Anodic Aluminum Oxide Membrane

**Yan Huang, Hong-yan Zeng*, Ce Zhao, Ye-qing Qu, and Pin Zhang**

College of Chemical Engineering, University of Xiangtan, Hunan 411105, China

(received date: 14 June 2010 / accepted date: 31 May 2011)

An anodized $Al_2O_3$ (AAO) membrane with apertures about 72 nm in diameter was prepared by two-step anodic oxidation. The appearance and pore arrangement of the AAO membrane were characterized by energy dispersive x-ray spectroscopy and scanning electron microscopy. It was confirmed that the pores with high pore aspect ratio were parallel, well-ordered, and uniform. The kinetics of pores growth in the AAO membrane was derived, and the kinetic models showed that pores stopped developing when the pressure ($\sigma$) trended to equal the surface tension at the end of anodic oxidation. During pore expansion, the effects of the oxalic acid concentration and expansion time on the pore size were investigated, and the kinetic behaviors were explained with two kinetic models derived in this study. They showed that the pore size increased with extended time ($r=G\cdot t+G'$), but decreased with increased concentration ($r=-K\cdot \ln c-K'$) through the derived mathematic formula. Also, the values of $G$, $G'$, $K$, and $K'$ were derived from our experimental data.

**Key words:** porous materials, alumina, anodization, electrochemistry, scanning electron microscopy(SEM)

## 1. INTRODUCTION

The process of aluminum anodization has received growing attention because anodic porous alumina templates are widely used for fabrication of various nanostructured materials. In the last decade, nanoporous anodic aluminum oxide (AAO) has become the object of much attention in various fields of research. Anodic oxidation of aluminum in various acid solutions causes a layer of aluminum oxide to form on the metal surface. This layer is characterized by parallel pores with orientations perpendicular to the sheet surface, and the pore aspect ratio (pore diameter vs. pore length) can reach values of 1:1 000 and more [1-5].

Porous anodic aluminum oxide is predominantly used as an important material in the fabrication of nanostructures. A number of studies have been performed in which the nanoporous structure is used as a template in the production of nanowires or nanotubes from various materials, such as carbon, metals, or polymers [6-10]. In addition, the porous membrane is used as a filter [11,12]. The adhesion of substances to the pore walls has also been used in some biosensor applications [13,14]. Another approach is to use the filtration capacities of nanoporous aluminum oxide for purification of DNA or whole cells from blood [15,16]. Furthermore, alumina is already a well-known material in orthopedic surgery and dentistry. Here, it is normally used with smoothed surfaces and has already proven biocompatible [17].

There has been a great deal of work investigating the structure, nature, and properties of AAOs in recent decades [18-23]. Takhistov and Biosens [24] studied mass-transfer at the nanoporous substrate by electrochemical impedance spectroscopy. Patermarakis and Moussoutzanis [25] developed a kinetic model obtained at different bath temperatures and current densities of Al anodization. Sullivan and Wood [26] presented a model of self-organizing pore growth which was based on the electric field distribution at the pore tips. Together with other models proposed by the previous researchers [27], Singaraju *et al.* [28,29] developed a model for porous AAO formation under constant current conditions and a model under constant voltage anodization. Parkhutik and Shershulsky [30] explained the dependence of pore diameters and pore distances on applied voltage and electrolyte composition. However, little work on investigating the kinetics of pore growth (the specific mathematic relation of pore size vs. electrolyte concentration and pore size vs. expansion time) was reported. In our work, kinetics models were obtained by investigating the pore growth process in an AAO membrane and the specific mathematic relation of pore size to expansion time and electrolyte concentration.

*Corresponding author: hongyanzeng99@hotmail.com, hyzeng@xtu.edu.cn

## 2. EXPERIMENTAL PROCEDURES

### 2.1. Preparation of AAO membrane

A nanoporous aluminum membrane was prepared by anodization of aluminum. Aluminum sheets (99.999%, size of 100 mm × 50 mm × 0.5 mm) were annealed at 500 °C for 2 h in a high-purity $N_2$ atmosphere and then cooled in a furnace. To remove surface oil from the specimens, they were rinsed with absolute acetone and ethanol, respectively, and then dried after twice washing with deionized water. The samples were immersed in 4 wt% $H_2SO_4$ and 7 wt% $H_2CrO_4$ mixed solution (by volume of 1:1) at 70 °C for 2 min to remove the natural oxide membrane, and then immersed in 10 wt% NaOH at 20 °C for 15 s to neutralize acid substance residues on the surface of the Al sheets. The samples were dried after twice washing with deionized water, immersed in absolute ethanol at 25 °C for 3 min, and subsequently put into 60 wt% $HCLO_4$ ethanol solution ($HClO_4$: $C_2H_5OH$: $H_2O$ =4:4:2, v/v/v) at 30 °C to carry out electrochemical polishing at voltage of 2 to 3 V for 2 to 3 min. The polished samples were immersed in a 0.3 M oxalic acid solution under a current density of 4.0 mA/cm$^2$ for 2 h (first step of anodic oxidation). To remove the first oxide membrane, the samples were immersed in a mixed solution with a 1:1 volume ratio of 6 wt% $H_3PO_4$ and 1.8 wt% $H_2CrO_4$ at 40 °C for 15 h and then dried after washing with deionized water. The samples were immersed in oxalic acid solutions with various concentrations of oxalic acid at 40 °C under a constant voltage of 40.0 V for 9 h (second step of anodic oxidation). Finally, the samples were immersed in 5% $H_3PO_4$ (v/v) solution at 30 °C to make the pores broaden for a period of time, dried after washing with deionized water, and then annealed with a muffle at 900 °C for 1 h. Thus, the AAO membrane was obtained.

### 2.2. Characterization of AAO membrane

Scanning electron micrography (SEM) was carried out with a JEOL JSM-6700F instrument and energy dispersive x-ray spectroscopy (EDS) analysis was performed with a Noran SystemSix instrument. EDS was used to determine the elemental composition of the AAO membrane. The SEM photographs were analyzed by the software Image Pro. following the procedure reported by Xing [31]. The distribution of pore diameters could be obtained with the analysis.

## 3. RESULTS AND DISCUSSION

### 3.1 SEM/EDS analysis of nanoporous AAO membrane

The composition of the nanoporous AAO membrane was determined by EDS (Table 1 and Fig. 1). The results showed that Al and O elements in the membrane had an Al/O molar ratio of about 3/2 and mass ratio of about 8/9, indicating the sample composition was $Al_2O_3$. To determine the morphology and pore-size distribution of the AAO membrane, the surface of the AAO membrane was observed by SEM (Fig. 2). The pores in the AAO membrane were well-regulated hexagonal modules (Fig. 2A), well parallel (Fig. 2B) and perpendicular to the barrier layer (Fig. 2C), which is similar to the results obtained previously by Sui and Saniger [32]. Therefore, the membrane with regulated pores can be used for the preparation of highly ordered nanoarrays or nanotubes.

**Table 1.** Analysis of elements composing the AAO membrane

| Elements | Mass (%) | Atom (%) |
|---|---|---|
| O | 47.81 | 60.71 |
| Al | 52.19 | 39.29 |
| Total | 100.00 | 100.00 |

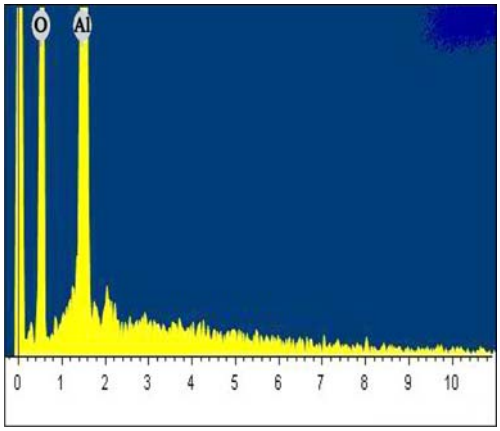


**Fig. 1.** EDS image of the AAO membrane.

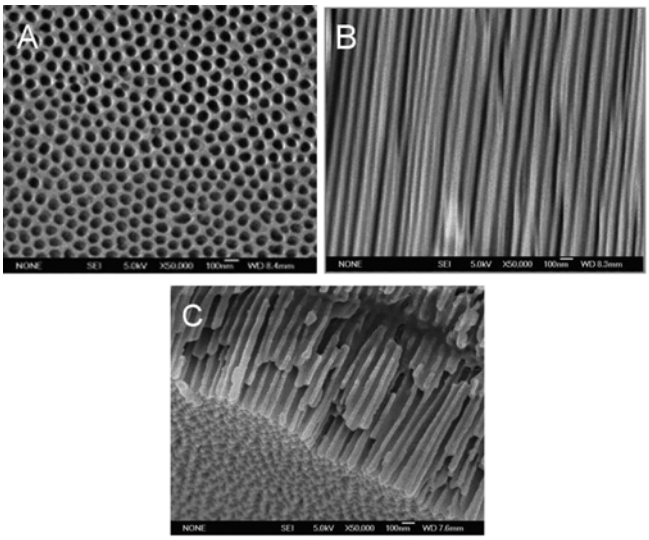


**Fig. 2.** SEM images of the AAO membrane A: top view; B: parallel nanopores; C: profile view (oxalic acid concentration of 0.3 M, voltage of 40 V, oxidation of 9 h and pore expansion time of 1 h).

### 3.2. Growth kinetics of AAO membrane

3.2.1. Growth process of pore in the AAO membrane

Under a high electric field, no electron but ions were conducted in the aluminum sheet, Therefore, the relation between the applied voltage and current density may be expressed as in [27] as

$$J=A\cdot\exp(B\frac{U}{d}), \tag{1}$$

where $J$ is the current density (mA/cm$^2$), $A$ and $B$ are parameters dependent on temperature which is determined by material physical property, $U$ is the applied voltage (V), and $d$ is the thickness of the barrier layer (nm).

In this process, the change of the electric charge distribution was much faster than that of the geometric size of the AAO membrane pores, so the process could be considered to be a state of quasi-static electric field. The pores on the AAO membrane grew lengthways, while they developed along the aperture under force of the electric field parallel to the aperture. The transverse electric field intensity is denoted as $E_x$ ($Ex<<E$, $E$ was total electric field intensity). The theory of electromagnetic field is given as

$$\omega=\frac{\varepsilon E_X^2}{8\pi}, \tag{2}$$

where $\omega$ is the density of the electrostatic field, and $\varepsilon$ is the dielectric constant of the membrane. Assuming that there is a small volume-element where the depth is $l$ and the area is $dS=2\pi r dr$, its electric field energy is

$$dA=\frac{\varepsilon E_X^2}{8\pi}\cdot 2\pi r dr\cdot l=\frac{\varepsilon E_X^2}{4}\cdot r dr\cdot l. \tag{3}$$

Therefore, the electrostatic force ($F$) along the aperture is

$$F=\frac{\partial A}{\partial r}=\frac{\varepsilon E_X^2}{4}\cdot r\cdot l, \tag{4}$$

and the pressure ($\sigma$) of the electrostatic field per depth is

$$\sigma=\frac{E}{L}=\frac{\varepsilon E_X^2}{4}\cdot r. \tag{5}$$

The value of the pressure increased linearly with increase in the square of $E_x$ and the instant pore diameter, while $E_x$ decreased with the increase of the pore diameter. The rate of $E_x$ decrease was higher than that of the pore diameter increase, so that $\sigma$ decreased with increase in the pore diameter. The pores stopped growing, and the pore size and the surface tension were dependent when the value of $\sigma$ was equal to the surface tension of the membrane. Hence, a large number of rounded pores with a similar diameter were formed (Figs. 4B and 7B), which was confirmed in the SEM and AFM images (Figs. 2A, 3Band 6B).

3.2.2. Kinetics of pore diameter to electrolyte concentration

The growth of the pores in the AAO membrane was not only related to the applied voltage, but also with electrolyte concentration and the time of pore expansion [33]. To examine the change of the pore diameter in various oxalic acid concentrations, an AAO membrane sample was prepared at 40 °C and 40 V after 9 h oxidation, and the pores in the membrane were un-expanded (Fig. 3). The pore size distribution curves for various concentrations of oxalic acid electrolyte are shown in Fig. 4. It was found that the pore diameter decreased with increasing oxalic acid concentrations. The

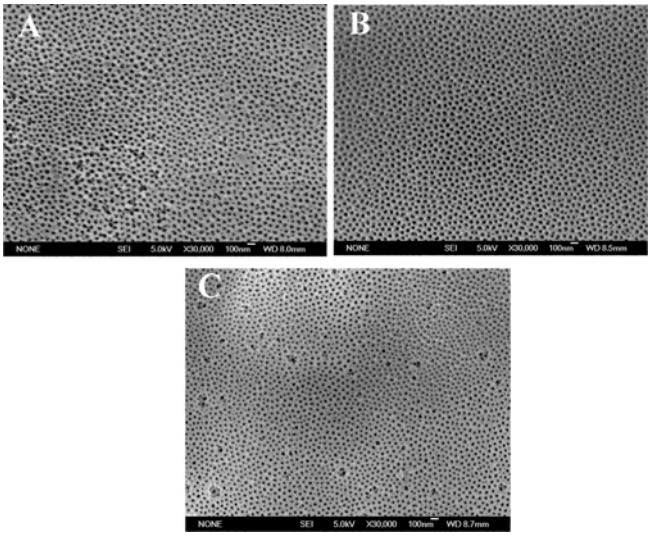


**Fig. 3.** SEM images of the AAO membrane under various oxalic acid concentrations, ×30,000, 40.0 V, 40.0 °C, 9 h, 0 h. A: 0.2 M; B: 0.3 M; C: 0.4 M.

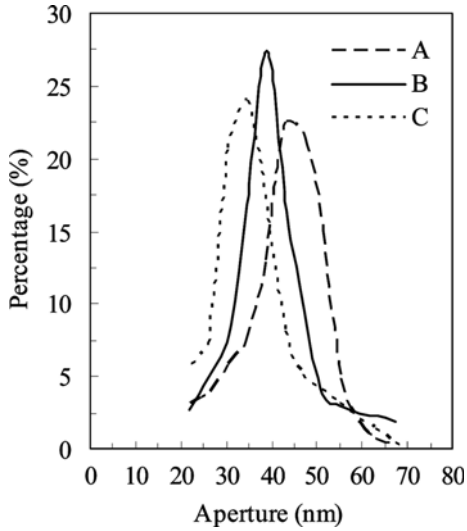


**Fig. 4.** Pore diameter distributions of the AAO membrane under various oxalic acid concentrations. A: 0.2 M; B: 0.3 M; C: 0.4 M.

AAO membrane in 0.3 M oxalic acid electrolyte showed the narrowest pore size distribution of about 39 nm (Fig. 4B), but the AAO membrane in 0.2 and 0.4 M oxalic acid electrolyte solutions had broader pore size distributions of about 45 nm (Fig. 4A) and 35 nm (Fig. 4C), respectively. The results were in agreement with SEM data (Fig. 5) calculated from SEM images (Fig. 3). It was likely because the current density was enhanced with increased oxalic acid concentrations, and the higher the current density, the smaller the aperture at the same voltage. When the concentration was 0.2 M, the pores of the AAO membrane were the largest but disordered (Fig. 3A). At 0.3 M, the pores grew smaller but were ordered and uniform (Fig. 3B). At 0.4 M, the aperture was the smallest and the pores were disordered, while there appeared to be some mergence between pores in the AAO membrane (Fig. 3C). The results showed that the pores were the most ordered and uniform at the concentration of 0.3 M. In addition, the effect of oxalic acid concentrations on aperture size was investigated at five concentrations, i.e. 0.1, 0.2, 0.3, 0.4, and 0.5 M. The data were plotted ln$X$ ($X$ was the oxalic acid concentration) versus aperture size to give a straight line with a high correlation coefficient ($R^2$=0.9973) (Fig. 5).

The pore size distribution curves for various pore expansion times for the AAO membrane are displayed in Fig. 7. The average pore size distributions in the AAO membrane with expansion times of 0, 1.0 and 1.5 h were 39, 72, and 89 nm, respectively. The pore size distribution in the AAO membrane for 1.0 h pore expansion was the narrowest at about 72 nm, but those for 0 and 1.5 h were broader from 20 nm to 80 nm and 50 nm to 110 nm, respectively. The results were similar to those in the SEM images (Fig. 6). Fig. 6 shows SEM images of the AAO membrane after various pore expansion times. The pores of the AAO membrane with un-expanded pores were oval, sparse, irregular, and small compared to

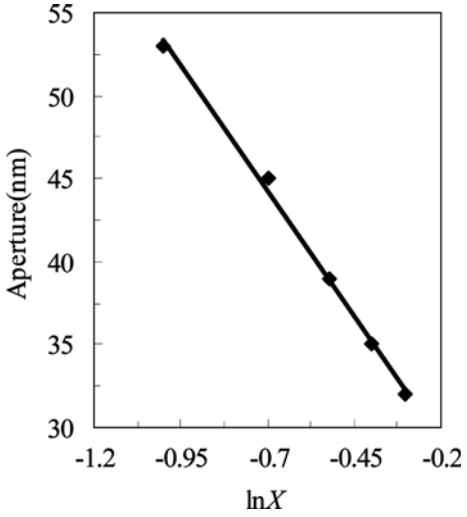


**Fig. 5.** Effect of oxalic acid concentrations on aperture size. $Y$= −30.316ln$X$+23.09, $Y$: aperture size; $X$: oxalic acid concentration.

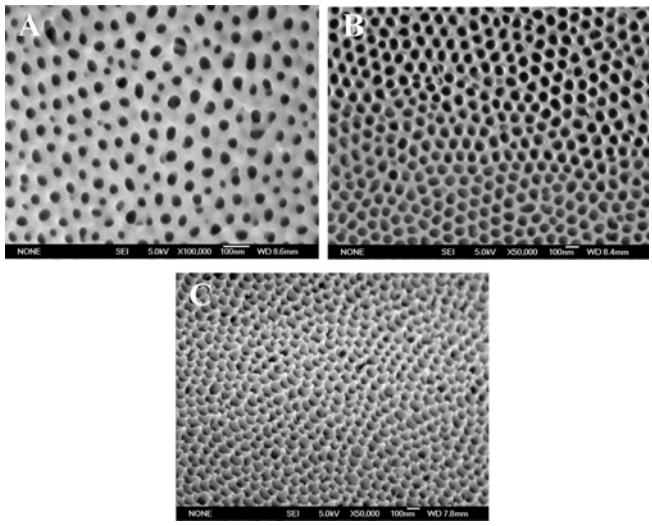


**Fig. 6.** SEM images of the AAO membrane with various pore expansion times. A: 0 h, ×100,000; B: 1.0 h, ×50,000; C: 1.5 h, ×50,000.

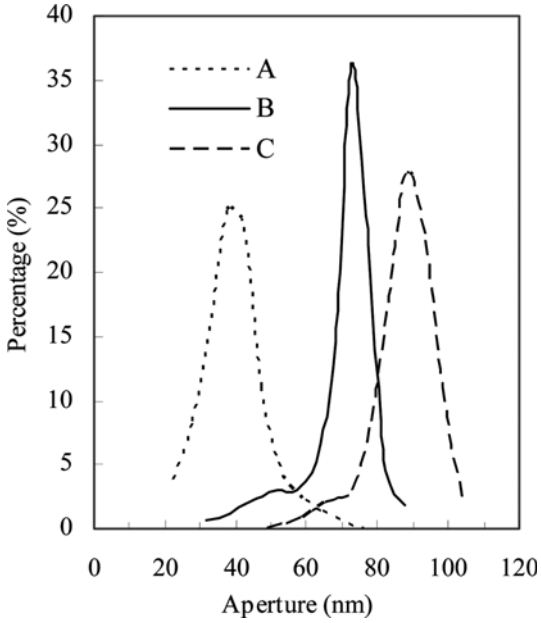


**Fig. 7.** Pore diameter distributions of the AAO membrane with various pore expansion times. A: 0 h, ×100,000; B: 1.0 h, ×50,000; C: 1.5 h, ×50,000.

those with expanded pore for 1 h (Figs. 6A and 6B). After 1.0 h of pore expansion, the pores were the most ordered and uniform, and almost round (Fig. 6B). After 1.5 h, the aperture was the largest and melting appeared on the surface of the AAO membrane (Fig. 6C). On the other hand, the effect of pore expansion time on aperture size was investigated for six periods of time, i.e. 0, 0.25, 0.5, 0.75, 1.0, and 1.5 h. The relation of aperture size to pore expansion time was linearly and significantly correlative ($R^2$=0.9996) (Fig. 8).

Generally, the pore size increased linearly with increase in the applied voltage within certain premises. To study other

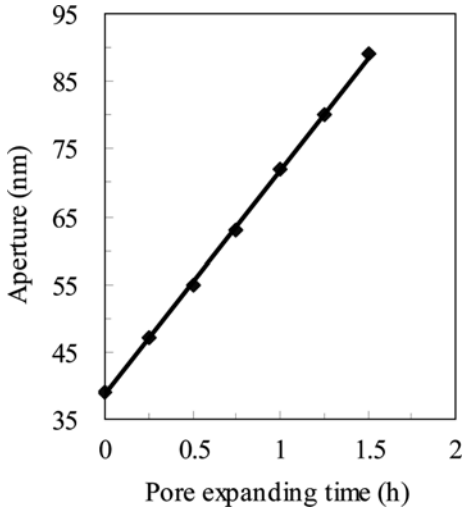


**Fig. 8.** Effect of pore expansion time on aperture size. $Y$=33.286$T$+38.607, $Y$: aperture size; $T$: pore expansion time.

factors which could influence pore growth, a model (eq. (6)) was selected for studying the profile of pore growth under pore expansion at 40 V constant voltage according to a previous study [33]:

$$m_1=k_1\cdot c\cdot t, \tag{6}$$

where $m_1$ is the mass of aluminum oxide, $c$ is the electrolyte concentration, $t$ is pore expansion time, and $k_1$ is a parameter dependent on applied voltage and temperature. According to the theorem of electrochemical reaction and mass conservation, the mass of the aluminum element is constant before and after oxidation of aluminum:

$$m=k_2\cdot m_1=k_3\cdot c\cdot \mathrm{t}, \tag{7}$$

$$\frac{\mathrm{d}m}{\mathrm{d}t}=k_3\cdot c, \tag{8}$$

where $m$ is the mass of aluminum before anodic oxidation, $k_2$=2$M$($Al$): $M$($Al_2O_3$)=54/102, and $k_3$=$k_1\cdot k_2$ ($M$ stands for molar mass). It serves as the basis for fitting to the Arrhenius equation:

$$\frac{\mathrm{d}m}{\mathrm{d}t}=\frac{M(Al)\cdot dC(Al)}{dt}=M(\mathrm{Al})\cdot A_1\cdot\exp(\frac{-E_a}{RT})=A\cdot\exp(\frac{-E_a}{RT}), \tag{9}$$

where $E_a$ is the activation energy, $R$ is the gas constant, and $T$ is the absolute temperature in Kelvin. Assuming the pores are constant in depth but change in diameter, according to the eq. (10) [34],

$$E_a=k_4\cdot r \tag{10}$$

where $r$ is the pore radius.

From eq. (8), (9) and (10),

$$k_3\cdot c=A\cdot\exp(\frac{-k_4\cdot r}{RT}) \tag{11}$$

is derived, and eq.(11) is simplified as

$$r=-\frac{RT}{k_4}\cdot\ln(k_3\cdot\frac{c}{A})=-\frac{RT}{k_4}\cdot\ln c-\frac{RT}{k_4}\cdot\ln(\frac{k_3}{A})=-K\cdot\ln c-K', \tag{12}$$

where $K=\frac{RT}{k_4}$, $K'=\frac{RT}{k_4}\cdot\ln(\frac{k_3}{A})$.

It is obvious in Fig. 5 that the pore diameter decreased with increase in oxalic acid concentrations in our experiment. A similar result was obtained for pore diameters changing with concentrations of a specific electrolyte in a previous study [35]. It was mainly due to dissimilar surface tensions in different concentrations of a specific electrolyte. Also, the pore size depended on the surface tension of the electrolyte during anodic oxidation before pore expansion (eq. (5)). Therefore, the pore size changed with different electrolytes as there were different surface tensions in different electrolytes. The kinetic model (eq. (12)) fitted to the experimental data (Fig. 5) for the relation between pore size and electrolyte concentration.

3.2.3. Kinetics of pore diameter vs. time

The following equation can be obtained according to the mass law:

$$m=\rho\pi r^2\cdot h \tag{13}$$

$$\frac{\mathrm{d}m}{\mathrm{d}t}=2\rho\pi rh\cdot\frac{\mathrm{d}r}{\mathrm{d}t}+\rho\pi r^2\cdot\frac{\mathrm{d}h}{\mathrm{d}t}, \tag{14}$$

where $\rho$ is the density of aluminum, $r$ is the pore radius, and $h$ is the pore depth. It was assumed that there was no change in pore depth during pore expansion, $\frac{\mathrm{d}h}{\mathrm{d}t}$=0. Therefore, eq. (14) can be reduced as

$$\frac{\mathrm{d}m}{\mathrm{d}t}=2\rho\pi rh\cdot\frac{\mathrm{d}r}{\mathrm{d}t}, \tag{15}$$

and it is obtained using eqs. (9), (10) and (15).

$$2\rho\pi rh\cdot\frac{\mathrm{d}r}{\mathrm{d}t}=A\cdot\exp(\frac{-k_4\cdot r}{RT}) \tag{16}$$

Equation (16) is simplified as

$$G_1\cdot\mathrm{d}t=r\cdot\exp(G_2\cdot r)\cdot\mathrm{d}r, \tag{17}$$

where $G_1=\frac{A}{2\rho\pi h}$ and $G_2=\frac{k_4}{RT}$.

$$G_1\cdot t=\frac{\left[r\cdot\exp(G_2\cdot r)-\frac{1}{G_2}\cdot\exp(G_2\cdot r)+\frac{1}{G_2}\right]}{G_2} \tag{18}$$

Moreover, exp($G_2\cdot r$) trended to 1. Because the pore was a

nanopore, ($G_2 \cdot r$) trended zero. Eq. (18) can be simplified as

$$r = G_1 \cdot G_2 \cdot t. \quad (19)$$

The pore size increased linearly with extended pore expansion time from eq. (19) when the $\frac{dh}{dt}$ was neglected (eq. (14)). Further analyzing the dependence in detail, eq. (19) was corrected to

$$r = G \cdot t + G' \quad (20)$$

where $G'$ was a modifier, while taking account of the effect of time on pore depth during pore expansion. The kinetic model (Eq. (20)) fitted to the experimental data (Fig. 8) for the relation of pore size to expansion time.

## 4. CONCLUSIONS

An AAO membrane with well-ordered and uniform pores was obtained by anodizing aluminum in an oxalic acid electrolyte by a two-step method. The kinetics of pore growth of a porous AAO membrane on aluminum sheets was investigated, and kinetic models based on electric-field-assisted growth were derived, which were proposed to understand the pore formation mechanism in the AAO membrane. The kinetic model showed that pores stopped developing when the pressure ($\sigma$) trended to equal the surface tension at the end of anodic oxidation. In the anodizing process, the effects of oxalic acid concentration and expansion time on the pore size were investigated. The kinetic models of aperture growth with various pore expansion times and oxalic acid concentrations were derived. They showed that pore size increased with extended expansion time (r=G·t+G'), but decreased with increased concentration (r=-K·lnc-K') through derived mathematic formula. Also, the values of G, G', K, and K' were derived from our experimental data.

## REFERENCES


1. C. R. Martin, *Science* **266**, 1961 (1994).
2. T. A. Hanaoka, A. Heilmann, M. Kroll, H. P. Kormann, T. Sawitowski, G. Schmid, P. Jutzi, A. Klipp, U. Kreibig, R. Neuendorf , *Appl. Organomet. Chem.* **12**, 367 (1998).
3. A. P. Li, F. Muller, A. Birner, K. Nielsch, and U. Gosele, *J. Appl. Phys.* **84**, 6023 (1998).
4. W. Lee, R. Scholz, K. Nielsch, and U. Gosele, *Angew. Chem. Int. Edit.* **44**, 6050 (2005).
5. H. Masuda, H. Asoh, M. Wabe, K. Nishio, M. Nakao, and T. Tamamura, *Adv. Mater.* **13**, 189 (2001).
6. J. Zhao, Q. Y. Gao, C. Gu, and Y. Yang, *Chem. Phys. Lett.* **358**, 77 (2002).
7. D. Lysenkov, H. Abbas, G. Muller, J. Engstler, K. P. Budna, J. J. Schneider, *J. Vac. Sci. Technol. B.* **23**, 809 (2005).
8. J. Choi, G. Sauer, K. Nielsch, R. B. Wehrspohn, and U. Gosele, *Chem. Mater.* **15**, 776 (2003).
9. M. Lahav, T. Sehayek, A. Vaskevich, and I. Rubinstein, *Angew. Chem. Int. Edit.* **42**, 5576 (2003).
10. M. Steinhart, J.H. Wendor, A. Greiner, R.B. Wehrspohn, K. Nielsch, J. Schilling, J. Choi, and U. Gösele, *Science* **296**, 1997 (2002).
11. A. Yamaguchi, F. Uejo, T. Yoda, T. Uchida, Y. Tanamura, T. Yamashita, and N. Teramae, *Nat. Mater.* **3**, 337 (2004).
12. A. Thormann, N. Teuscher, M. Pfannmçller, U. Rothe, and A. Heilmann, *Small* **3**, 1032 (2007).
13. A. Heilmann, N. Teuscher, A. Kiesow, D. Janasek, and U. Spohn, *J. Nanosci. Nanotechnol.* **3**, 375 (2003).
14. P. Takhistov, *Biosens Bioelectron*. **19**, 1445 (2004).
15. I. Vlassiouk, A. Krasnoslobodtsev, S. Smirnov, and M. Germann, *Langmuir.* **20**, 9913 (2004).
16. S. Dreve, E. Indrea, I. Bratu, M. Bako, G. H. Mihailescu, L. Olenic, Stela, Pruneanu, V. Znamirovschi, and L. Barbu-Tudoran, *Physica*, Special Issue. **1**, 381 (2003).
17. S. F. Hulbert, in An Introduction to Bioceramics, L. L. Hench, and J. Wilson, (eds.), *World Scientific*, pp. 25-40, Singapore (1993).
18. X. W. Wang, G. T. Fei, X. J. Xu, Z. Jin, and L. D. Zhang, *J. Phys. Chem. B.* **109**, 24326 (2005).
19. Y. Matsui, K. Nishio, and H. Masuda, *Small.* **2**, 522 (2006).
20. L. Zhang, P. Zhang, and Y. Fang, *Anal. Chim. Acta.* **591**, 214 (2007).
21. F. Zhang, L. Yang, S. Bi, J. Liu, F. Liu, X. Wang, X. Yang, N. Gan, T. Yu, J. Hu, H. Li, and T. Yang, *J. Inorg. Biochem.* **87**, 105 (2001).
22. G. Chen, A. S. Soper, and R. L. McCarley, *Langmuir.* **23**, 11777 (2007).
23. W. Zhang, Z. Huang, J. Yu, D. Gao, J. Qian, *J. Biomedical Engineering* **22**, 1007 (2005).
24. P. Takhistov and Biosens, *Bioelectron*. **19**, 1445 (2004).
25. G. Patermarakis and K. Moussoutzanis, *J. Electrochem. Soc.* **142**, 737 (1995).
26. P. O. Sullivan and G. C. Wood, *P. Roy. Soc. A-Math. Phy.* **317**, 511 (1970).
27. G. E. Thompson and G. C. Wood, *Nature* **290**, 230 (1981).
28. R. Kanakla, P. V. Singaraju, R.Venkat, and B. Das, *J. Electrochem. Soc.* **152**, J1-J5 (2005).
29. P. Singaraju, R. Venkat, R. Kanakla, B. Das, *Phys. Appl. Phys.* **35**, 107 (2006).
30. V. P. Parkhutik, and V. I. Shershulsky, *J. Phys. B-At. Mol. Opt.* **25**, 1258 (1992).
31. Z. Xing, G. Wu, S. Huang, S. Chen, and H. Zeng, *J. Supercrit. Fluid.* **47**, 281 (2008).
32. Y. Sui and J. M. Saniger, *Mater. Lett.* **48**, 127 (2001).
33. A. Jagminas and D. Bigelien, *J. Cryst. Growth* **233**, 591 (2001).
34. Y. Gong , W. Wang, H. Wang, and H. Guo, *Acta. Phys-Chim. Sin.* **20**, 199 (2004).
35. R. Rocio, A. Vazquez-Olmos, M. E. Mata-Zamora, A. Ordonez-Medrano, F. Rivera-Torres, and J. M. Saniger, *J. Colloid. Interf. Sci.* **287**, 664 (2005).